CENTRE FOR **STOCHASTIC GEOMETRY**
AND ADVANCED **BIOIMAGING**

Francisco Cuevas-Pacheco and Jesper Møller

Log Gaussian Cox processes on the sphere

No. 04, March 2018

Log Gaussian Cox processes on the sphere

Francisco Cuevas-Pacheco and Jesper Møller

Department of Mathematical Sciences, Aalborg University

Abstract

We define and study the existence of log Gaussian Cox processes (LGCPs) for the description of inhomogeneous and aggregated/clustered point patterns on the d-dimensional sphere, with $d = 2$ of primary interest. Useful theoretical properties of LGCPs are studied and applied for the description of sky positions of galaxies, in comparison with previous analysis using a Thomas process. We focus on simple estimation procedures and model checking based on functional summary statistics and the global envelope test.

Keywords: Hölder continuity, minimum contrast estimation, model checking, point processes on the sphere, reduced Palm distribution, second order intensity reweighted homogeneity.

1 Introduction

Statistical analysis of point patterns on the sphere have been of interest for a long time (e.g. Pebles, 1974; Pebles and Groth, 1975; Ripley, 1977; Bahcall and Soneira, 1981; Scott and Tout, 1989; Raskin, 1994; Robeson et al., 2014; Lawrence et al., 2016; Møller and Rubak, 2016). Although models and methods developed for planar and spatial point processes may be adapted, statistical methodology for point processes on the sphere is still in its infancy.

Recently, the focus has been on developing functional summary statistics and parametric models. For homogeneous point patterns, Robeson et al. (2014) studied Ripley's K-function on the sphere (Ripley, 1976, 1977), and Lawrence et al. (2016) provided a careful presentation of Ripley's K-function and other functional summary statistics such as the empty space function F, the nearest-neighbour distance function G, and the $J = (1 - G)/(1 - F)$ function, including how to account for edge effects. See also Møller and Rubak (2016) for details and the connection to reduced Palm distributions. For inhomogeneous point patterns, Lawrence et al. (2016) and Møller and Rubak (2016) studied the pair correlation function and the inhomogeneous K-function. The models which have been detailed are rather scare: Homogeneous Poisson point process models (Raskin, 1994; Robeson et al., 2014), inhomogeneous Poisson point process models and Thomas point process models for aggregated/clustered point patterns (Lawrence et al., 2016; Section 2.2–2.3 in the

present paper), and determinantal point processes (Møller and Rubak, 2016; Møller et al., 2018) for regular/repulsive point patterns.

This paper concerns inhomogeneous aggregated/clustered point patterns on the sphere and studies how the theory of log Gaussian Cox processes (LGCP Møller et al., 1998) can be adapted to analysing such data. In particular, we demonstrate that an inhomogeneous LGCP provides a better description of the sky positions of galaxies analysed in Lawrence et al. (2016) by using an inhomogeneous Thomas process. For comparison, as in Lawrence et al. (2016), we use a minimum contrast procedure for parameter estimation, where we discuss the sensibility of the choice of user-specified parameters. No model checking was done for the fitted inhomogeneous Thomas process in Lawrence et al. (2016). We show how a thinning procedure apply to generate homogeneous point patterns so that the F, G, J-functions can be used for model checking.

The paper is organised as follows. Section 2 provides the setting and needed background material on point processes, particularly on Poisson and Cox processes, the data example of sky positions of galaxies, and the inhomogeneous Thomas process introduced in Lawrence et al. (2016). Section 3 contains the definition and existence conditions for LGCPs on the sphere, studies their useful properties, and compares the fitted Thomas processes and LGCPs for the data example. Finally, Section 4 summarizes our results and discusses future directions for research.

2 Background

2.1 Setting

Let $\mathbb{S}^d = \{x \in \mathbb{R}^{d+1} : \|x\| = 1\}$ denote the d-dimensional unit sphere included in the $(d+1)$-dimensional Euclidean space $\mathbb{R}^{d+1}$, equipped with the usual inner product $\langle x, y\rangle = \sum_{i=0}^{d} x_i y_i$ for points $x = (x_0, \ldots, x_d), y = (y_0, \ldots, y_d) \in \mathbb{R}^{d+1}$ and the usual length $\|x\| = \sqrt{\langle x, x\rangle}$. We are mainly interested in the case of $d = 2$. For unit vectors $u, v \in \mathbb{S}^d$, let $d(u, v) = \arccos(\langle u, v\rangle)$ be the geodesic distance on the sphere.

By a point process on $\mathbb{S}^d$, we understand a random finite subset $\mathbf{X}$ of $\mathbb{S}^d$. We say that $\mathbf{X}$ is isotropic if $O\mathbf{X}$ is distributed as $\mathbf{X}$ for any $(d+1) \times (d+1)$ rotation matrix O. We assume that $\mathbf{X}$ has an intensity function, $\lambda(u)$, and a pair correlation function, $g(u, v)$, meaning that if $U, V \subseteq \mathbb{S}^d$ are disjoint regions on the sphere and $N(U)$ denotes the cardinality of $X \cap U$, then

$$\mathrm{E}[N(U)] = \int_U \lambda(u)\,\mathrm{d}u, \qquad \mathrm{E}[N(U)N(V)] = \int_U \int_V \lambda(u)\lambda(v)g(u, v)\,\mathrm{d}u\,\mathrm{d}v,$$

where $\mathrm{d}u$ is the Lebesgue/surface measure on $\mathbb{S}^d$. We say that $\mathbf{X}$ is (first order) homogeneous if $\lambda(u) = \lambda$ is constant, and second order intensity reweighted homogeneous if $g(u, v) = g(r)$ only depends on $r = d(u, v)$. Note that these properties are implied by isotropy of $\mathbf{X}$, and second order intensity reweighted homogeneity allows to define the (inhomogeneous) K-function (Baddeley et al., 2000) by

$$K(r) = \int_0^r g(s)\,\mathrm{d}s, \qquad r \geq 0. \tag{2.1}$$

2.2 Poisson and Cox processes

For a Poisson process $\mathbf{X}$ on $\mathbb{S}^d$ with intensity function λ, $N(\mathbb{S}^d)$ is Poisson distributed with mean $\int \lambda(u)\,\mathrm{d}u$ and the points in $\mathbf{X}$ are independent identically distributed with a density proportional to λ. The process is second order intensity reweighted homogeneous, with K-function

$$K_{\mathrm{Pois}}(r) = 2\pi(1-\cos r) \qquad \text{if } d = 2. \tag{2.2}$$

Let $\mathbf{Z} = \{\mathbf{Z}(u) : u \in \mathbb{S}^d\}$ be a non-negative random field so that almost surely $\int \mathbf{Z}(u)\,\mathrm{d}u$ is well-defined and finite, and each random variable $\mathbf{Z}(u)$ has finite variance. We say that $\mathbf{X}$ is a Cox process driven by $\mathbf{Z}$ if $\mathbf{X}$ conditional on $\mathbf{Z}$ is a Poisson process on $\mathbb{S}^d$ with intensity function $\mathbf{Z}$. Setting $0/0 = 0$, define the residual driving random field by $\mathbf{Z}_0 = \{\mathbf{Z}_0(u) : u \in \mathbb{S}^d\}$ where $\mathbf{Z}_0(u) = \mathbf{Z}(u)/\lambda(u)$. Then the intensity function and pair correlation function are

$$\lambda(u) = \mathbb{E}[\mathbf{Z}(u)], \qquad g(u,v) = \mathbb{E}\left[\mathbf{Z_0}(u)\mathbf{Z_0}(v)\right]. \tag{2.3}$$

Thus $\mathbf{X}$ is second order intensity reweighted homogeneous if $\mathbf{Z}_0$ is isotropic, that is, $\{\mathbf{Z}_0(Ou) : u \in \mathbb{S}^d\}$ is distributed as $\mathbf{Z}_0$ for any $(d+1)\times(d+1)$ rotation matrix O. We shall naturally specify such Cox processes in terms of λ and $\mathbf{Z}_0$.

2.3 Data example and inhomogeneous Thomas process

Figure 1a shows the sky positions of 10 546 galaxies from the Revised New General Catalogue and Index Catalogue (RNGC/IC) (Steinicke, 2015). Here, we are following Lawrence et al. (2016) in making a rotation of the original data so that the two circles limit a band around equator, which is an approximation of the part of the sky obscured by the Milky Way, and the observation window $W \subset \mathbb{S}^2$ is the complement of the band; 64 galaxies contained in the band are omitted.

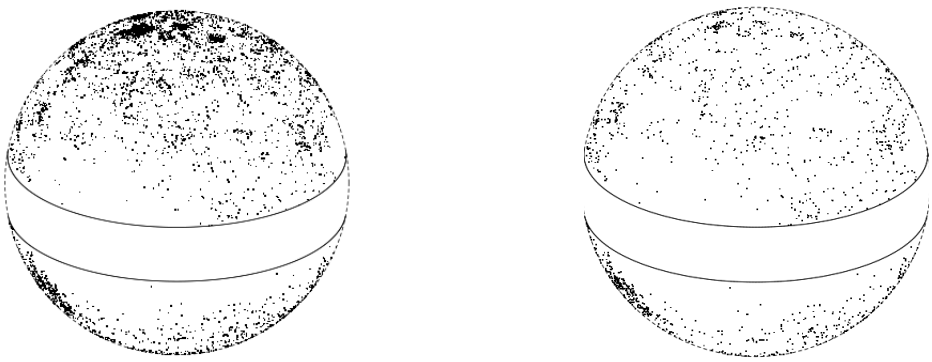

(a) Sky positions of galaxies before thinning. **(b)** Sky positions of galaxies after thinning.

Figure 1: The sky positions of (a) 10 546 galaxies and (b) 3285 galaxies obtained after a thinning procedure so that a homogeneous point pattern is expected to be obtained. The circles limit the part of the sky obscured by the Milky Way.

Different plots and tests in the accompanying supporting information to Lawrence et al. (2016) clearly show that the galaxies are aggregated and not well-described by an inhomogeneous Poisson process model. Lawrence et al. (2016) fitted

the intensity function

$$\lambda(u) = 6.06 - 0.112 \sin\theta\cos\phi - 0.149 \sin\theta\sin\phi + 0.320\cos\theta + 1.971\cos^2\theta, \quad (2.4)$$

where $u = (\sin\theta\cos\phi, \sin\theta\sin\phi, \cos\theta)$, $\theta \in [0, \pi]$ is the colatitude, and $\phi \in [0, 2\pi)$ is the longitude. Throughout this paper, we use this estimate.

Lawrence et al. (2016) proposed an inhomogeneous Thomas process, that is, a Cox process with intensity function (2.4) and isotropic residual driving random field given by

$$\mathbf{Z}_0(u) = \sum_{y \in \mathbf{Y}} f_{y,\xi}(u)/\kappa, \qquad u \in \mathbb{S}^2, \quad (2.5)$$

where $\mathbf{Y}$ is a homogeneous Poisson process on $\mathbb{S}^2$ with intensity $\kappa > 0$, and where

$$f_{y,\xi}(u) = \frac{\xi}{4\pi \sinh\xi} \exp(\xi\langle u, y\rangle), \qquad u \in \mathbb{S}^2,$$

is the density for a von Mises-Fisher distribution on $\mathbb{S}^2$ with mean direction y and concentration parameter $\xi > 0$. They estimated κ and η by a minimum contrast procedure (Diggle and Gratton, 1984; Diggle, 2013), where a non-parametric estimate $\widehat{K}$ is compared to

$$K(r) = K_{(\kappa,\eta)}(r) = K_{\mathrm{Pois}}(r) + \frac{\cosh(2\xi) - \cosh\bigl(\sqrt{2\xi^2(1+\cos r)}\bigr)}{4\kappa \sin^2\xi}.$$

Specifically, the minimum contrast estimate $(\hat{\kappa}, \hat{\eta})$ is minimising the contrast

$$\int_a^b \bigl(\widehat{K}(r)^{0.25} - K_{(\kappa,\eta)}(r)^{0.25}\bigr)^2 \,\mathrm{d}r, \quad (2.6)$$

where $b > a \geq 0$ are user-specified parameters. Lawrence et al. (2016) used the integration interval $[a, b] = [0, 1.396]$, where 1.396 is the maximal value of the smallest distance from the north pole respective south pole to the boundary of W. They obtained $\hat{\kappa} = 5.64$ and $\hat{\xi} = 266.6$.

3 Log Gaussian Cox processes

3.1 Definition and existence

Let $\mathbf{Y} = \{\log \mathbf{Y}(u) : u \in \mathbb{S}^d\}$ be a Gaussian random field (GRF), that is, $\sum_{i=1}^n a_i \mathbf{Y}(u_i)$ is normally distributed for any integer $n > 0$, numbers $a_1, \ldots, a_n$, and $u_1, \ldots, u_n \in \mathbb{S}^d$. Let $\mu(u) = \mathrm{E}\mathbf{Y}(u)$ be its mean function and $c(u, v) = \mathrm{E}[(\mathbf{Y}(u) - \mu(u))(\mathbf{Y}(v) - \mu(v))]$ its covariance function. Assuming that almost surely $\mathbf{Z} := \exp(\mathbf{Y})$ is integrable, the Cox process $\mathbf{X}$ driven by $\mathbf{Z}$ is called a log Gaussian Cox process (LGCP; Møller et al., 1998; Møller and Waagepetersen, 2004).

Define the corresponding mean-zero GRF, $\mathbf{Y}_0 := \mathbf{Y} - \mu$, which has also covariance function c, and let $\mathbf{X}_0$ be the LGCP driven by $\mathbf{Z}_0 := \exp(\mathbf{Y}_0)$. Assuming μ is a Borel function with an upper bounded, then almost sure continuity of $\mathbf{Z}_0$ implies almost

sure integrability of $\mathbf{Z}$, and so $\mathbf{X}$ is well-defined. In turn, almost sure continuity of $\mathbf{Z}_0$ is implied if almost surely $\mathbf{Y}_0$ is locally sample Hölder continuity of some order $k > 0$, which means the following: With probability one, for every $s \in \mathbb{S}^d$, there is a neighbourhood V of s and a constant $C_{V,k}$ so that

$$\sup_{u,v \in V, u \neq v} \left| \frac{\mathbf{Y}_0(u) - \mathbf{Y}_0(v)}{d(u,v)^k} \right| \leq C_{V,k}. \tag{3.1}$$

The following proposition, which follows from Lang et al. (2016, Corollary 4.5), provides a simple condition ensuring (3.1).

Proposition 3.1. *Let*

$$\gamma(u,v) = \mathbb{E}[(\mathbf{Y}_0(u) - \mathbf{Y}_0(v))^2]$$

be the variogram of a mean-zero GRF $\mathbf{Y}_0$*. Suppose there exists numbers* $s \in (0,1]$*,* $\ell \in (0,1)$*, and* $m > 0$ *such that*

$$\gamma(u,v) \leq m\, d(u,v)^{\ell/2} \qquad \text{whenever } d(u,v) < s. \tag{3.2}$$

Then, for any $k \in (0, \ell/2)$*, almost surely* $\mathbf{Y}_0$ *is locally sample Hölder continuous of order* k*.*

3.2 Properties

The following proposition is verified along similar lines as Proposition 5.4 in Møller and Waagepetersen (2004) using (2.3) and the expression for the Laplace transform of a normally distributed random variable.

Proposition 3.2. *A LGCP* $\mathbf{X}$ *has intensity function and pair correlation functions given by*

$$\lambda(u) = \exp(\mu(u) + c(u,u)/2), \qquad g(u,v) = \exp(c(u,v)), \tag{3.3}$$

where μ *and* c *are the mean and covariance functions of the underlying GRF.*

In other words, the distribution of $\mathbf{X}$ is specified by (λ, g) because $\mu(u) = \log \lambda(u) - \log g(u,u)/2$ and $c(u,v) = \log g(u,v)$ specify the distribution of the GRF. Proposition 3.2 extends as follows. For a general point process on $\mathbb{S}^d$, the n-th order pair correlation function $g(u_1, \ldots, u_n)$ is defined for integers $n \geq 2$ and multiple disjoint regions $U_1 \ldots, U_n \subseteq \mathbb{S}^d$ by

$$\mathrm{E}\left[N(U_1) \cdots N(U_n)\right] = \int_{U_1} \cdots \int_{U_n} \lambda(u_1) \cdots \lambda(u_n)\, g(u_1, \ldots, u_n)\, \mathrm{d}u_1 \cdots \mathrm{d}u_n$$

provided this multiple integral is well-defined and finite. For the LGCP, this is the case for any n and

$$g(u_1, \ldots, u_n) = \exp\Big(\sum_{1 \leq i < j \leq n} c(u_i, u_j) \Big). \tag{3.4}$$

This follows as in Møller and Waagepetersen (2003, Theorem 1).

By (3.3), second order intensity reweighted homogeneity of the LGCP is equivalent to isotropy of the covariance function, that is, $c(u,v) = c(r)$ depends only on $r = d(u,v)$. Parametric classes of isotropic covariance functions on $\mathbb{S}^d$ are provided by Gneiting (2013) and Møller et al. (2018). In this paper, we use the so-called multiquadric covariance function which is isotropic and given by

$$c_{(\sigma,\delta,\tau)}(r) = \sigma^2 \left(\frac{(1-\delta)^2}{1+\delta^2-2\delta\cos r} \right)^{\tau}, \qquad r \in [0,\pi], \tag{3.5}$$

where $(\sigma,\delta,\tau) \in (0,\infty)\times(0,1)\times(0,\infty)$.

Proposition 3.3. *A mean-zero GRF $\mathbf{Y}_0$ with multiquadric covariance function is locally sample Hölder continuous of any order $k \in (0,1)$.*

Proof. By (3.5), for $r = d(u,v)$,

$$\gamma(u,v) = 2c_{(\sigma,\delta,\tau)}(0) - 2c_{(\sigma,\delta,\tau)}(r) = 2\sigma^2\left(1 - c_{(1,\delta,1)}(r)^{\tau}\right). \tag{3.6}$$

Here, letting $p = 2\delta/(1+\delta^2)$,

$$\begin{aligned} c_{(1,\delta,1)}(r) &= \frac{(1-\delta)^2}{1+\delta^2-2\delta\cos r} = \frac{1-p}{1-p\cos r} \\ &= 1 + p\left(\frac{\cos r - 1}{1-p\cos r}\right) \geq 1 + p(\cos r - 1) \\ &\geq 1 - pr^2/2, \end{aligned} \tag{3.7}$$

where the first inequality follows from $0 < p < 1$ because $0 < \delta < 1$, and the second inequality follows from $1 - \cos x \leq x^2/2$ whenever $0 \leq x \leq 1$. If $\tau < 1$, then

$$\gamma(u,v) \leq 2\sigma^2\big(1 - c_{(1,\delta,1)}(r)\big) \leq p\sigma^2 r^2,$$

where the first inequality follows from (3.6) and the second from (3.7). If $\tau \geq 1$, then for any $\alpha \in (0,2]$,

$$\gamma(u,v) \leq 2\sigma^2\big(1 - (1-pr^2/2)^{\tau}\big) \leq p\sigma^2\tau r^2 \leq p\sigma^2\tau r^{\alpha},$$

where the first inequality follows from (3.6)-(3.7) and the second from $1-(1-x)^{\tau} \leq x\tau$ whenever $0 \leq x \leq 1$. Hence, for any $(\sigma,\delta,\tau) \in (0,\infty)\times(0,1)\times(0,\infty)$ and any $\alpha \in (0,2)$, (3.5) satisfies (3.2) with $s = 1$, $\ell = 2\alpha$, and $m = p\sigma^2\tilde{\tau}$, where $\tilde{\tau} = \max(1,\tau)$. □

Incidentally, a word about the reduced Palm distribution of $\mathbf{X}$ at a given point $u \in \mathbb{S}^d$. Intuitively, this is the distribution of $\mathbf{X} \setminus \{u\}$ conditional on that $u \in \mathbf{X}$; see Lawrence et al. (2016) and Møller and Rubak (2016). Along similar lines as in Coeurjolly et al. (2017, Theorem 1), we obtain the following result.

Proposition 3.4. *Consider a LGCP $\mathbf{X}$ those underlying GRF has mean and covariance functions μ and c. For any $u \in \mathbb{S}^d$, the reduced Palm distribution of $\mathbf{X}$ at u is a LGCP where the underlying GRF has mean function $m_u(v) = m(v) + c(u,v)$ and unchanged covariance function c.*

3.3 Comparison of fitted Thomas processes and LGCPs for the data example

In this section, to see how well the estimated Thomas process, $\mathbf{X}_{\text{Thom}}$ say, obtained in Lawrence et al. (2016) fits the sky positions of galaxies discussed in Section 2.3, we use methods not involving the K-function (or the related pair correlation function, cf. (2.1)) because it was used in the estimation procedure.

The point pattern in Figure 1b was obtained by an independent thinning procedure of the point pattern in Figure 1a, with retention probability $\lambda_{\min}/\lambda(u)$ at location $u \in W$, where $\lambda(u)$ is given by (2.4) and $\lambda_{\min} = \inf_{u \in W} /\lambda(u)$. Thus the corresponding thinned Thomas process, $\mathbf{X}_{\text{thinThom}}$ say, is homogeneous so that the F, G, J-functions apply (see Section 1 and the references therein). Empirical estimates $\widehat{F}, \widehat{G}, \widehat{J}$ can then be used as test functions for the global rank envelope test, which is supplied with graphical representations of global envelopes for $\widehat{F}, \widehat{G}, \widehat{J}$ as described in Myllymäki et al. (2017). As we combined all three test functions as discussed in Mrkvička et al. (2016) and Mrkvička et al. (2017), we followed their recommendation of using $3 \times 2499 = 7497$ simulations of $\mathbf{X}_{\text{thinThom}}$ for the calculation of p-values and envelopes. In Table 1, the limits of the p-intervals correspond to liberal and conservative versions of the global rank envelope test (Myllymäki et al., 2017). Table 1 and Figure 2a–2c clearly show that the estimated Thomas process is not providing a satisfactory fit no matter if in the contrast (2.6) the long integration interval $[a, b] = [0, 1.396]$ from Lawrence et al. (2016) or the shorter interval $[a, b] = [0, 0.175]$ (corresponding to 0-10 degrees) is used for parameter estimation. When $[a, b] = [0, 0.175]$, larger estimates $\hat{\kappa} = 6.67$ and $\hat{\xi} = 353.94$ are obtained as compared to $\hat{\kappa} = 5.64$ and $\hat{\xi} = 266.6$ from Lawrence et al. (2016). Note that the p-values and envelopes are not much affected by the choice of integration interval in the minimum contrast estimation procedure, cf. Table 1 and Figure 2a–2c. The envelopes indicate that at short inter-point distances r, there is more aggregation in the data than expected under the two fitted Thomas processes.

Table 1: Intervals for p-values obtained from the global envelope test based on combining the F, G, J-functions and using either a short or long integration interval $[a, b]$ when calculating the contrast used for parameter estimation in the Thomas process or the LGCP.

	$[a, b] = [0, 0.175]$	$[a, b] = [0, 1.396]$
Thomas process	0.01% – 1.05%	0.01% – 1.28%
LGCP	24.02% – 24.09%	0.01% – 1.23%

We also fitted an inhomogeneous LGCP, $\mathbf{X}_{\text{LGCP}}$ say, still with intensity function given by (2.4) and with multiquadric covariance function as in (3.5). The same minimum contrast procedure as above was used except of course that in the contrast given by (2.6), the theoretical K-function was obtained by combining (2.1), (3.3), and (3.5), where numerical calculation of the integral in (2.1) was used. The estimates are $(\hat{\sigma}^2, \hat{\delta}, \hat{\tau}) = (4.50, 0.99, 0.25)$ if $[a, b] = [0, 0.175]$ is the integration interval, and $(\hat{\sigma}^2, \hat{\delta}, \hat{\tau}) = (1.30, 0.87, 2.03)$ if $[a, b] = [0, 1.396]$. For each choice of integration interval, Figure 3 shows the estimated log pair correlation function, that is, the esti-

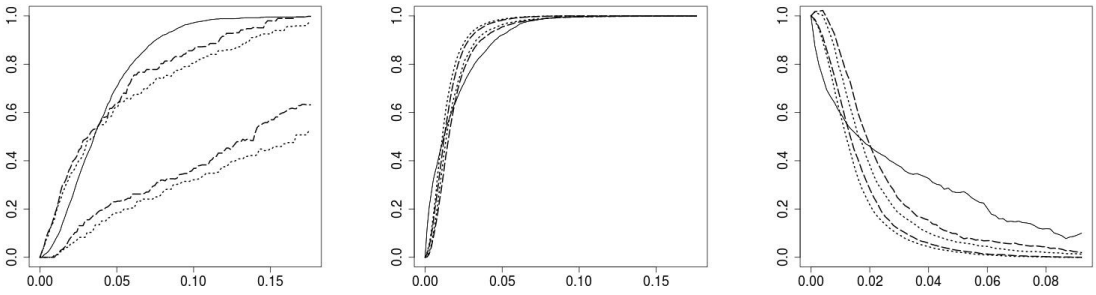

(a) F-function (Thomas). **(b)** G-function (Thomas). **(c)** J-function (Thomas).

(d) F-function (LGCP). **(e)** G-function (LGCP). **(f)** J-function (LGCP).

Figure 2: Empirical functional summary statistics and 95% global envelopes under (a)–(c) fitted Thomas process and (d)–(f) fitted LGCPs for the sky positions of galaxies after thinning. The solid lines show $\widehat{F}(r), \widehat{G}(r), \widehat{J}(r)$ versus distance r (measured in radians). The dotted and dashed lines limit the global envelopes and correspond to the short and long integration intervals $[a, b] = [0, 0.175]$ and $[a, b] = [0, 1.396]$, respectively, used in the minimum contrast estimation procedure.

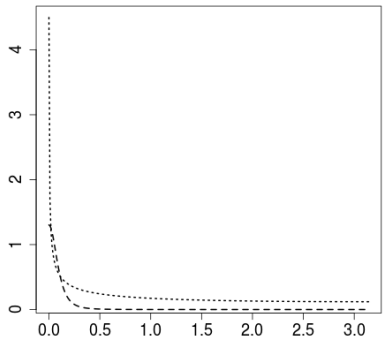

Figure 3: Plot of estimated pair correlation functions $g(r)$ (on a logarithmic scale) versus $r \in [0, \pi]$ for the LGCP when different integration intervals $[a, b]$ were used in the minumum contrast estimation procedure (dotted line: $[a, b] = [0, 0.175]$; dashed line: $[a, b] = [0, 1.396]$).

mated covariance function of the underlying GRF, cf. (3.3). Comparing the two pair correlation functions, the one based on the short integration interval is much larger for very short inter-point distances r, then rather similar to the other at a short interval of r-values, and afterwards again larger, so the fitted LGCP using the short integration interval is more aggregated than the other case. Further, Figure 4 shows the empirical K-function and the fitted K-functions for both the Thomas process and the LGCP when using the different integration intervals (for ease of comparison, we have subtracted K_{Pois}, the theoretical K-function for a Poisson process, cf.(2.2)). The fitted K-functions are far away from the empirical K-function for large values of r. However, having a good agreement for small and modest values of r is more important, because the variance of the empirical K-function seems to be an increasing function of r and the interpretation of the K-function becomes harder for large r-values. For small and modest r-values, using the LGCP model and the short integration interval provides the best agreement between the empirical K-function and the theoretical K-function, even when r is outside the short integration interval.

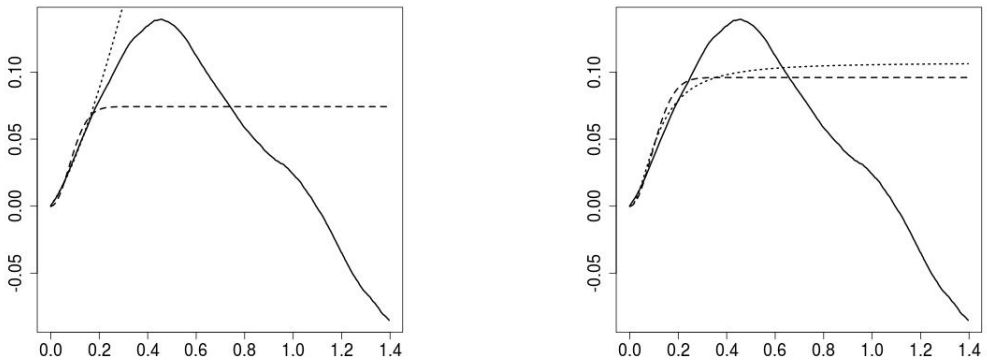

(a) Integration interval [0,0.175]. **(b)** Integration interval [0,1.396].

Figure 4: Fitted K-functions minus the theoretical Poisson K-function versus distance r for the sky positions of galaxies when using different integration intervals in the minumum contrast estimation procedure. The solid lines correspond to the empirical functional summary statistics, and the dashed and dotted lines correspond to the theoretical functional summary statistics under the fitted Thomas processes and LGCPs, respectively.

Table 1 and Figure 2d–2f show the results for the fitted LGCPs when making a model checking along similar lines as for the fitted Thomas processes (i.e., based on a thinned LGCP and considering the empirical F, G, J-functions together with global envelopes). Table 1 shows that the fitted LGCP based on the long integration interval gives an interval of similar low p-values as for the fitted Thomas process in Lawrence et al. (2016), and Figure 2e–2f indicate that the data is more aggregated than expected under this fitted LGCP. Finally, the fitted LGCP based on the short integration interval gives p-values of about 24%, and the empirical curves of the functional summary statistics appear in the center of the envelopes, cf. Figure 2d–2f.

4 Concluding remarks

As demonstrated in this paper, a LGCP on the sphere possesses useful theoretical properties, in particular moment properties and a simple characterization of the reduced Palm distribution as another LGCP. We exploited the expressions for the intensity and pair correlation function when dealing with the inhomogeneous K-function, which concerns the second moment properties of a second order intensity reweighted homogeneous point process. Higher-order pair correlation functions as given by (3.4) may be used for constructing further functional summaries e.g. along similar lines as the third-order characteristic studied in Møller et al. (1998). It would also be interesting to exploit the result for the reduced Palm distribution as discussed in Coeurjolly et al. (2017).

For comparison with the analysis of the sky positions of galaxies in Lawrence et al. (2016), we used a minimum contrast estimation procedure, but other simple and fast methods such as composite likelihood (Guan, 2006; Møller and Waagepetersen, 2017, and the references therein) could have been used as well. It is well-known that such estimation procedures can be sensitive to the choice of user-specified parameters. We demonstrated this for the choice of integration interval in the contrast, where using a short interval and an inhomogeneous LGCP provided a satisfactory fit, in contrast to using an inhomogeneous Thomas process or a long interval. It could be interesting to use more advanced estimation procedures such as maximum likelihood and Bayesian inference. This will involve a time-consuming missing data simulation-based approach (Møller and Waagepetersen, 2004, 2017, and the references therein).

The Thomas process is a mechanistic model since it has an interpretation as a cluster point process (Lawrence et al., 2016). The original Thomas process in $\mathbb{R}^3$ (i.e., using a 3-dimensional isotropic zero-mean normal distribution as the density for a point relative to its cluster centre) may perhaps appear natural for positions of galaxies in the 3-dimensional space – but we question if the Thomas process from Lawrence et al. (2016) is a natural model for the sky positions because these points are obtained by projecting clusters of galaxies in space to a sphere which may not produce a clear clustering because of overlap. Rather, we think both the inhomogeneous Thomas and the inhomogeneous LGCP should be viewed as empirical models for the data. Moreover, it could be investigated if the Thomas process replaced by another type of Neyman-Scott process (Neyman and Scott, 1958, 1972) or a (generalised) shot noise Cox process (Møller, 2003; Møller and Torrisi, 2005) would provide an adequate fit.

As a specific model, we only considered the multiquadric covariance function for the underlying GRF of the LGCP. A more flexible model could be the spectral model studied in Møller et al. (2018), where a parametric model for the eigenvalues of the spectral representation of an isotropic covariance function $c(r)$ ($r \geq 0$) in terms of spherical harmonics is used (incidentally, the eigenvalues are also known for the multiquadric covariance function if $\tau = 1/2$). The spectral representation allows a Karhunen-Loève representation which could be used for simulation. However, for the data analysed in this paper, we found it easier and faster just to approximate the GRF $\mathbf{Y} = \{\mathbf{Y}(u) : u \in \mathbb{S}^2\}$, using a finite grid $I \subset \mathbb{S}^2$ so that each $\mathbf{Y}(u)$ is

replaced by $\mathbf{Y}(v)$ if v is the nearest grid point to u, and using the singular value decomposition when simulating the finite random field $\{\mathbf{Y}(v) : v \in I\}$. When using spherical angles (θ, ψ) as in (2.4), a regular grid over $[0, \pi] \times [0, 2\pi)$ can not be recommended, since the density of grid points will large close to the poles and small close to equator. Using a regular grid $I \subset \mathbb{S}^2$ avoids this problem, nonetheless, there are only five regular grids on the sphere (Coxeter, 1973). We used a nearly-regular grid consisting of 4098 points on the sphere (Szalay et al., 2007, and the references therein) and computed using the R package `mvmesh` (Nolan, 2016).

Acknowledgements

Supported by The Danish Council for Independent Research | Natural Sciences, grant DFF – 7014-00074 "Statistics for point processes in space and beyond", and by the "Centre for Stochastic Geometry and Advanced Bioimaging", funded by grant 8721 from the Villum Foundation.

References

A. J. Baddeley, J. Møller, and R. Waagepetersen. Non- and semi-parametric estimation of interaction in inhomogeneous point patterns. *Statistica Neerlandica*, 54:329–350, 2000.

J. N. Bahcall and R. M. Soneira. The distribution of stars to v = 16th magnitude near the north galactic pole: normalization, clustering properties and counts in various bands. *Astrophysical Journal*, 246:122–135, 1981.

J.-F. Coeurjolly, J. Møller, and R. Waagepetersen. Palm distributions for log Gaussian Cox processes. *Scandinavian Journal of Statistics*, 44:192–203, 2017.

H. S. M. Coxeter. *Regular Polytopes*. Methuen, London, 1973.

P. J. Diggle. *Statistical Analysis of Spatial and Spatio-temporal Point Patterns*. CRC Press, Boca Raton, 2013.

P. J. Diggle and R. J. Gratton. Monte Carlo methods of inference for implicit statistical models. *Journal of the Royal Statistical Society: Series B (Statistical Methodology)*, 46: 193–227, 1984.

T. Gneiting. Strictly and non-strictly positive definite functions on spheres. *Bernoulli*, 19: 1327–1349, 2013.

Y. Guan. A composite likelihood approach in fitting spatial point process models. *Journal of the American Statistical Association*, 101:1502–1512, 2006.

A. Lang, J. Potthoff, M. Schlather, and D. Schwab. Continuity of random fields on Riemannian manifolds. Manuscript available at arXiv: 1607.05859, 2016.

T. Lawrence, A. Baddeley, R. K. Milne, and G. Nair. Point pattern analysis on a region of a sphere. *Stat*, 5:144–157, 2016.

J. Møller. Shot noise Cox processes. *Advances in Applied Probability*, 35:614–640, 2003.

J. Møller and E. Rubak. Functional summary statistics on the sphere with an application to determinantal point processes. *Spatial Statistics*, 18:4–23, 2016.

J. Møller and G. Torrisi. Generalised shot noise Cox processes. *Advances in Applied Probability*, 37:48–74, 2005.

J. Møller and R. Waagepetersen. Some recent developments in statistics for spatial point patterns. *Annual Review of Statistics and Its Applications*, 4:317–342, 2017.

J. Møller and R. P. Waagepetersen. *Spatial Statistics and Computational Methods*, chapter An introduction to simulation-based inference for spatial point processes, pages 37–60. Lecture Notes in Statistics 173, Springer-Verlag, New York, 2003.

J. Møller and R. P. Waagepetersen. *Statistical Inference and Simulation for Spatial Point Processes*. Boca Raton, FL, Chapman & Hall/CRC., 2004.

J. Møller, R. Waagepetersen, and A. R. Syversveen. Log Gaussian Cox processes. *Scandinavian Journal of Statistics*, 25:451–482, 1998.

J. Møller, M. Nielsen, E. Porcu, and E. Rubak. Determinantal point process models on the sphere. *Bernoulli*, 24:1171–1201, 2018.

T. Mrkvička, S. Soubeyrand, M. Myllymäki, P. Grabarnik, and U. Hahn. Monte Carlo testing in spatial statistics, with applications to spatial residuals. *Spatial Statistics*, 18: 40–53, 2016.

T. Mrkvička, M. Myllymäki, and U. Hahn. Multiple Monte Carlo testing, with applications in spatial points. *Statistics and Computing*, 27:1239–1255, 2017.

M. Myllymäki, T. Mrkvička, P. Grabarnik, H. Seijo, and U. Hahn. Global envelope tests for spatial processes. *Journal of the Royal Statistical Society: Series B (Statistical Methodology)*, 79:381–404, 2017.

J. Neyman and E. L. Scott. Statistical approach to problems of cosmology. *Journal of the Royal Statistical Society: Series B (Statistical Methodology)*, 20:1–43, 1958.

J. Neyman and E. L. Scott. *Processes of Clustering and Applications*. John Wiley & Sons, New York, Stochastic Processes in Lewis PAW edition, 1972.

J. P. Nolan. An R package for modeling and simulating generalized spherical and related distributions. *Journal of Statistical Distributions and Applications*, 3:3–14, 2016.

P. J. E. Pebles. The nature of the distribution of galaxies. *Astronomy and Astrophysics*, 32:197–202, 1974.

P. J. E. Pebles and E. J. Groth. Statistical analysis of catalogs of extragalactic objects. v. three point correlation function for the galaxy distribution in the Zwicky catalog. *Astrophysical Journal*, 196:1–11, 1975.

R. G. Raskin. Spatial analysis on the sphere: a review, 1994. NGCIA technical report. (Available from `http://eprints.cdlib.org/uc/item/5748n2xz`). [Accessed February 1, 2018].

B. D. Ripley. The second-order analysis of spatial point processes. *Journal of Applied Probability*, 13:255–266, 1976.

B. D. Ripley. Modelling spatial patterns (with discussion). *Journal of the Royal Statistical Society: Series B (Statistical Methodology)*, 39:172–212, 1977.

S. M. Robeson, A. Li, and C. Huang. Point-pattern analysis on the sphere. *Spatial Statistics*, 10:76–86, 2014.

D. Scott and C. A. Tout. Nearest neighbour analysis of random distributions on a sphere. *Monthly Notices of the Royal Astronomical Society*, 241:109–117, 1989.

W. Steinicke. Revised new general catalogue and index catalogue, 2015. (Available from `http://www.klima-luft.de/steinicke/index.htm`). [Accessed February 1, 2018].

A. S. Szalay, J. Gray, G. Fekete, P. Z. Kunszt, P. Kukol, and A. Thakar. Indexing the sphere with the hierarchical triangular mesh. Manuscript available at arXiv: 0701164, 2007.